EDGE ARTICLE

Check for updates

Macroscopic handedness inversion of terbium coordination polymers achieved by doping homochiral ligand analogues†

Chang-Yu Wang, Jia-Ge Jia, Guo-Guo Weng, Ming-Feng Qin, Kui Xu and Li-Min Zheng [ID] *

Inspired by natural biological systems, chiral or handedness inversion by altering external and internal conditions to influence intermolecular interactions is an attractive topic for regulating chiral self-assembled materials. For coordination polymers, the regulation of their helical handedness remains little reported compared to polymers and supramolecules. In this work, we choose the chiral ligands R-pempH$_2$ (pempH$_2$ = (1-phenylethylamino)methylphosphonic acid) and R-XpempH$_2$ (X = F, Cl, Br) as the second ligand, which can introduce C−H···π and C−H···X interactions, doped into the reaction system of the Tb(R-cyampH)$_3$·3H$_2$O (cyampH$_2$ = (1-cyclohexylethylamino)methylphosphonic acid) coordination polymer, which itself can form a right-handed superhelix by van der Waals forces, and a series of superhelices R-1H-x, R-2F-x, R-3Cl-x, and R-4Br-x with different doping ratios x were obtained, whose handedness is related to the second ligand and its doping ratio, indicating the decisive role of interchain interactions of different strengths in the helical handedness. This study could provide a new pathway for the design and self-assembly of chiral materials with controllable handedness and help the further understanding of the mechanism of self-assembly of coordination polymers forming macroscopic helical systems.

Introduction

Chirality transcription and inversion are among the most sophisticated processes in biological systems which can ensure dynamic control of structure and function.[1] Artificial helical nanostructures with controllable chirality are attractive for the development of materials with outstanding properties such as chiral recognition,[2] asymmetric catalysis,[3] and circularly polarized luminescence.[4] Since chiral transfer and amplification from the molecular to the macroscopic level is realized through intermolecular interactions, which are susceptible to changes under internal or external conditions, chirality inversion is possible and has been realized in some supramolecular assemblies and polymers.[5] This phenomenon is quite intriguing because chirality inversion makes it possible to generate superhelices of opposite chirality from the same chiral molecules under different external or internal conditions, such as solvents,[6] pH,[7] achiral additives,[8] metal ions,[9] temperatures,[10] and others.[11] Notably, although the use of dopants to induce

chirality has been well explored in supramolecular systems, they are not specific to macroscopic helical systems. As far as we are aware, there are two methods to control the macroscopic handedness of molecular materials by doping. One is that chiral dopants can induce chirality in otherwise achiral supramolecular systems,[12] and the other is that achiral molecules are doped and co-assembled with chiral molecules, causing handedness inversion in chiral supramolecular self-assemblies.[13] In the latter case, the type and doping ratio of achiral molecules can affect the handedness of the self-assemblies.[8b,14] Nevertheless, in these supramolecular examples, (1) the synthesis of organic molecules usually requires tedious synthetic steps; (2) the complex intermolecular interactions especially in the presence of dopants also pose great difficulties in the mechanism study of chirality inversion, which in turn makes it difficult to predict and design new handedness-regulating systems.

Unlike supramolecular assemblies, which consist of small molecular building blocks through noncovalent interactions, coordination polymers (CPs) are composed of metal ions and organic linkers through coordination bonds. Different combinations of metal ions and organic ligands can form CPs with a variety of structures and interesting physicochemical properties.[15] Therefore, studying the chirality transfer and inversion of CPs can greatly expand the applications of chiral materials. It is noticed, however, that most of the chiral CPs reported so far are in the form of crystalline materials.[16] Only in a few cases,

State Key Laboratory of Coordination Chemistry, School of Chemistry and Chemical Engineering, Collaborative Innovation Centre of Advanced Microstructures, Nanjing University, Nanjing 210023, P. R. China. E-mail: lmzheng@nju.edu.cn

† Electronic supplementary information (ESI) available: Experimental details and full characterization studies of all described compounds. See DOI: https://doi.org/10.1039/d3sc03230b

homochiral CPs with helical morphology have been realized.[17–19] Our previous studies on Ln/R- or S-pempH$_2$ systems [Ln = Tb, Gd; pempH$_2$ = (1-phenylethylamino)methylphosphonic acid] have demonstrated that the assembly of one-dimensional (1D) chiral CPs in crystal and helical forms provides insight into the mechanisms of chiral transcription and amplification from molecule to morphology, and chirality inversion may be achieved by intentionally regulating inter-chain interactions by using pH and counteranions.[18]

In this work, we present an innovative strategy to invert the macroscopic chirality of 1D CPs by doping ligand analogues into the assemblies. We chose a Tb/R- or S-cyampH$_2$ [cyampH$_2$ = (1-cyclohexylethyl)aminomethylphosphonic acid] system for this study because the reaction of Tb(OAc)$_3$·3H$_2$O and R- or S-cyampH$_2$ produces superhelices of R- or S–Tb(cyampH)$_3$·3H$_2$O, whose morphology is attributed to the conformer interconversion of cyclohexyl groups and weak interchain van der Waals interaction.[19] The structures of the superhelices are closely related to those of R- or S-Tb(cyampH)$_3$·HOAc·2H$_2$O crystals with 1D chain structures (Fig. 1). Since the interchain interactions in Tb(R-cyampH)$_3$·3H$_2$O superhelices are governed by van der Waals forces, they can be modulated by ligand doping to introduce other weak interactions. Thus, the Tb/R-cyampH$_2$ system provides an excellent platform for studying the critical role of doping-induced interchain interactions in the macro-scopic chirality of 1D chiral CPs, while avoiding the deficiency of the supramolecular system where the mechanism is often unclear due to the complexity of intermolecular interactions.

By doping the Tb/R-cyampH$_2$ system with R-pempH$_2$ ligands at different ratios (5–20%), we obtained superhelices of R–Tb(cyampH)$_{3(1-a)}$(pempH)$_{3a}$·3H$_2$O (R-1H-x, x is the doping ratio of pempH$_2$ into the reaction system and a is the actual ratio of pempH$_2$ in the product; $x \approx a$). Interestingly, the chirality of the superhelices was found to depend on the amount of doped pempH$^-$ ligand (Scheme 1). When x = 0–6%, the superhelix is purely right-handed (P); when x = 9–20%, it is purely left-handed (M); and when x is between 7% and 8%, both left and right-handed superhelices are present. Halogen substituted ligands such as FpempH$_2$ and ClpempH$_2$ are found to have a similar effect on the chirality inversion as well. But for BrpempH$_2$, the resulting superhelices are all right-handed when
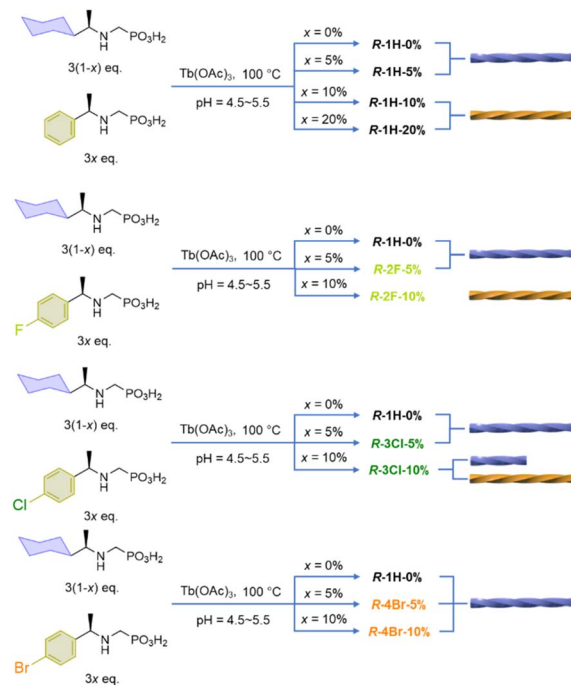
Scheme 1 The synthesis of R-pempH$_2$ and R-XpempH$_2$-doped superhelices.

x = 5% and 10%. This is the first report on the use of the doping method to achieve macroscopic chirality inversion of CP aggregates. Our work not only adds a new element to the toolbox of various external stimuli that can achieve helical inversion, but also broadens the intersection of the fields of macroscopic helical assembly and CP chemistry.

Results and discussion

Synthesis and characterization of pempH$_2$-doped superhelices

Since the superhelices of Tb(R-cyampH)$_3$·3H$_2$O (R-1H-0%) can be obtained by hydrothermal reaction between Tb(OAc)$_3$ and R-cyampH$_2$ (ref. 20) at pH 4.3–6.5 and 80–140 °C, we chose similar reaction conditions to synthesize the doped superhelices R-1H-x (x = 5%, 10% or 20%). The molar ratio of the lanthanide salt to the sum of the two ligands was kept as 1 : 3, and the ratio of R-cyampH$_2$ to R-pempH$_2$ was determined according to the value of the doping ratio of R-pempH$_2$ (x). After the hydrothermal reaction at pH 5.0 and 100 °C for 1 day and cooling to room temperature, the precipitates on the bottom of the vessel were collected by centrifugation, washed with water several times, and dried in air. The morphologies of R-1H-x products can be examined by scanning electron microscopy (SEM). As shown in Fig. 2, all the products have a helical shape with diameters in the range of 200 nm to 2 μm and lengths ranging from 2 to 40 μm, while superhelices of R-1H-5% with less doped R-pempH$_2$ ligand were right-handed (P); meanwhile, superhelices of R-1H-10% and R-1H-20% with more doped R-pempH$_2$ ligand were left-handed (M). It is noteworthy that their sizes were much smaller than those of undoped R-1H-0% superhelices (Table 1).
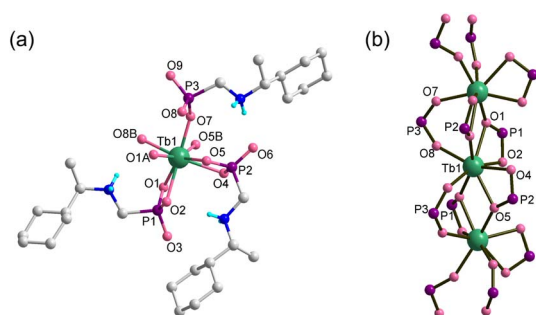

Fig. 1 (a) Building unit with atomic labeling and (b) single chain structure of Tb(R-cyampH)$_3$·HOAc·2H$_2$O. The organic groups are omitted in (b) for clarity.
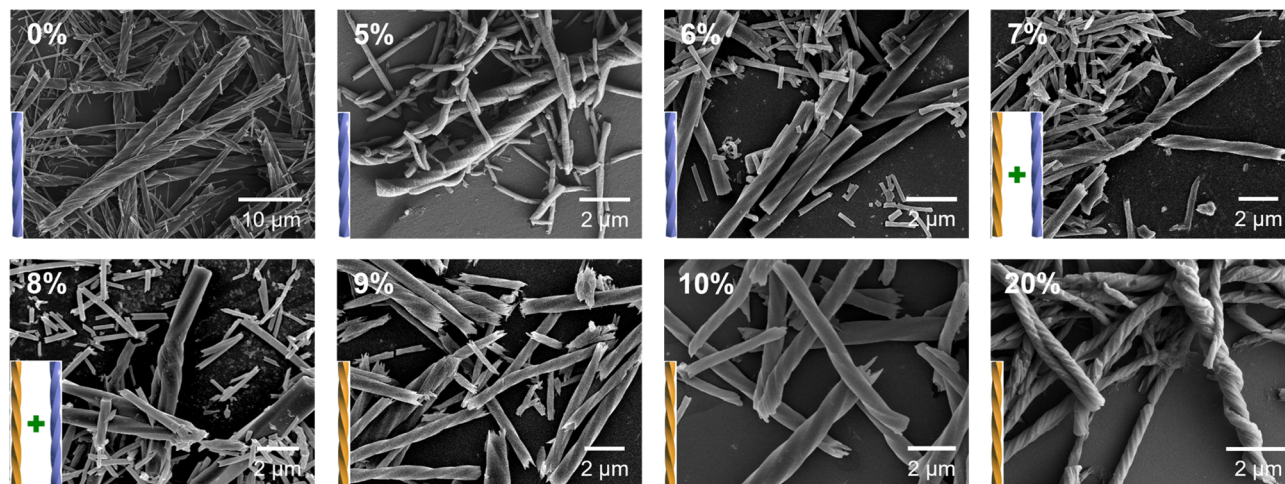
Fig. 2 SEM images of *R*-1H-*x* (*x* = 0–20%) obtained *via* the hydrothermal reaction at pH 5.0 and 100 °C for 1 day.

Table 1 The actual formulae of compounds *R*-1H-*x* obtained at pH 5.0 and 100 °C. The ratios of the two ligands were calculated by using the integrals of signal peaks in their ^{1}H-NMR spectra. The photoluminescence lifetimes and quantum yields are given for comparison

Compound	The actual formula	Ratio[a] (*a*)	Handedness	Diameter (μm)	Length (μm)	Lifetime[b] (ms)	Quantum yield (%)
R-1H-0%	Tb(*R*-cyampH)$_3$	0%	Superhelix (*P*)	2–7	40–100	3.27	10.51
R-1H-5%	Tb(*R*-cyampH)$_{2.80}$(*R*-pempH)$_{0.20}$·3H$_2$O	6.5%	Superhelix (*P*)	0.2–1	2–20	3.59	35.11
R-1H-10%	Tb(*R*-cyampH)$_{2.61}$(*R*-pempH)$_{0.39}$·3H$_2$O	12.9%	Superhelix (*M*)	0.2–2	2–25	3.53	34.79
R-1H-20%	Tb(*R*-cyampH)$_{2.41}$(*R*-pempH)$_{0.59}$·3H$_2$O	19.8%	Superhelix (*M*)	0.2–1	2–15	3.44	30.48

[a] The ratio is determined by using ^{1}H NMR spectra. [b] λ_{em} = 543 nm.

The handedness inversion that occurs from doping ratio *x* = 5% to 10% triggered our curiosity about what would happen when *x* is between 5% and 10%. Therefore, we prepared the complexes *R*-1H-6% to *R*-1H-9% at pH = 5.0, which were treated under the same hydrothermal conditions. The SEM images showed that superhelices of *R*-1H-6% were all right-handed as *R*-1H-5%, and superhelices of *R*-1H-9% were all left-handed as *R*-1H-10% as well. When *x* was 7% or 8%, both right-handed and left-handed superhelices were observed, while right-handed superhelices were predominant in *R*-1H-7% but relatively rare in *R*-1H-8% (Fig. 2). Nearly no straight rods were observed under the field of view of an electron microscope. These results indicated that the chirality inversion happened just in a narrow range of the doping ratio *x* between 7% and 8%.

Although handedness inversion occurred as an increasing amount of *R*-pempH$_2$ was doped into the system, the helical products shared the same crystal structures as *R*-1H-0%, which were verified by their identical powder X-ray diffraction (PXRD) patterns (Fig. 3c). Like *R*-1H-0%, *R*-1H-*x* (*x* = 5%, 10%, 20%) showed broad diffraction peaks at 2θ = 6.0, 10.4, 12.0, and 15.9°. The diffraction peaks were indexed by using TOPAS 5.0,[21] yielding a set of unit cell parameters in space group *P*6$_5$ of *a* = 17.01 Å, *c* = 23.53 Å and *V* = 5898.8 Å^3 for all *R*-1H-5%, 10% and 20% products (Fig. S1–S3†).

The infrared (IR) spectra may show the presence of the *R*-pempH$_2$ ligand in *R*-1H-*x*. As shown in Fig. 3a, the IR spectra of *R*-1H-*x* are nearly the same. However, there is one difference that can be noticed in these IR spectra, which is a weak peak at 702 cm^{-1} in *R*-1H-*x* (Fig. 3b). It is attributed to the out-of-plane bending vibration of the phenyl group and its strength increases with the increasing doping amount of the *R*-pempH$_2$ ligand (Fig. S4†). The same trend was also observed in the luminescence spectra. Theoretically, the doped *R*-pempH$_2$ ligand has a more effective capacity sensitizing the *f–f* transition of Tb^{3+} than the non-aromatic *R*-cyampH$_2$ ligand. Therefore, *R*-1H-*x* with a value of *x* ≥ 5% should emit more intense luminescence than undoped *R*-1H-0%. This was confirmed by the luminescence spectra of *R*-1H-*x* upon excitation at 257 nm which showed significant emission bands peaking at 489, 543, 583, and 621 nm (Fig. S5†), corresponding to the *f–f* transitions of Tb^{3+} from ^{5}D$_4$ to ^{7}F$_J$ (*J* = 6, 5, 4 and 3). To quantitatively study the effect of the doping ratio on the luminescence, we measured the quantum yield and lifetime of the stimulated emission of *R*-1H-*x* products. Their lifetimes (τ) of emission at 543 nm are all in the range of 3.2–3.6 ms and their quantum yields (Φ) are 10–35% (Table 1 and Fig. S6†). The increase in quantum yield from *R*-1H-0% to *R*-1H-5% and *R*-1H-10% is consistent with the stronger ability of the *R*-pempH$_2$ ligand to sensitize the *f–f* transition of Tb^{3+} centers. Meanwhile, the decrease in quantum yield of *R*-1H-20% may be attributed to the aggregation-induced quenching (ACQ) effect caused by more *R*-pempH$_2$ ligands in the CP system.
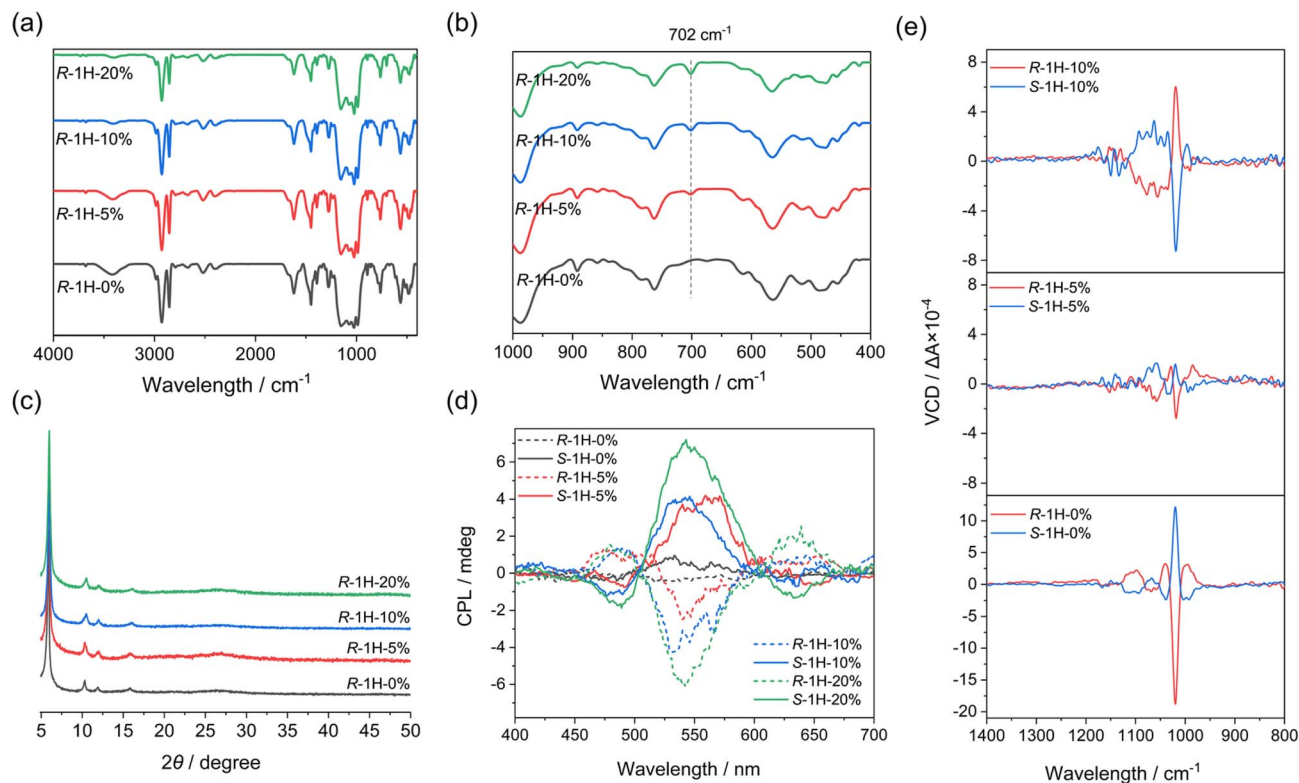
Fig. 3 IR spectra (4000–400 cm^{-1} (a) and 1000–400 cm^{-1} (b)), PXRD patterns (c) of **R**-1H-x obtained at pH 5.0 with different x values (x = 0%, 5%, 10%, 20%), and CPL spectra (d) and VCD spectra (e) of **R**- and **S**-1H-x obtained at pH 5.0 (x = 0%, 5%, 10%).

Both the IR and the luminescence spectra confirmed the presence of the R-pempH$_2$ ligand in the products, and the R-pempH$_2$ content increased with the doping ratio. The above results demonstrate that **R-1H-x** superhelices exhibit almost the same structure as **R-1H-0%**, but part of R-cyampH$_2$ was replaced by R-pempH$_2$ in **R-1H-x**. Combined with the results of elemental analysis, energy dispersive X-ray analysis (EDX) (Fig. S7†), and TG analyses (Fig. S8a†), we propose that the molecular formulae of **R-1H-x** are R–Tb(cyampH)$_{3(1-a)}$(pempH)$_{3a}$·3H$_2$O.

In order to further determine the actual ratio (a) of R-pempH$_2$ in **R-1H-x** superhelices, we used ^{1}H-NMR spectroscopy to analyze the component of **R-1H-x** digested in acid. The ^{1}H-NMR spectra of **R-1H-x** (x = 0%, 5%, 10%, and 20%) which were dissolved in DMSO-d$_6$ solutions containing 1M D$_2$SO$_4$ showed the peaks of hydrogen atoms from the R-cyampH$_2$ ligand and relatively weaker peaks corresponding to hydrogen atoms of the R-pempH$_2$ ligand (Fig. S9–S12†). The positions of these peaks are consistent with those in the ^{1}H-NMR spectra of the two pure ligands. These positions and their attributions of the ^{1}H-NMR signal peaks are described in the experimental section. We chose the peaks that were farther away from other strong peaks for the calculation to reduce the inaccuracy of peak area integration. For the R-cyampH$_2$ ligand, the signal peak suitable for the calculation is the multiplet at $\delta = 3.18$, which is attributed to the hydrogen atoms of the methylene (–CH$_2$) and methine (–CH) groups; and for the R-pempH$_2$ ligand the peak is the quartet at $\delta = 4.40$, which is attributed to the hydrogen atoms of the methine (–CH) group. The calculation results, as

shown in Table 1, showed that the actual molar ratios (a) of the R-pempH$_2$ ligand to the total ligands in **R-1H-x** matched quite well with the doping ratios (x).

The chirality of pempH$_2$-doped superhelices

To check whether the doping of the S-pempH$_2$ ligand has the opposite effect to its enantiomer, similar experiments were also performed with S-cyampH$_2$ and S-pempH$_2$ (x = 5%, 10%, 20%). As expected, **S-1H-5%** obtained at pH 5.0 showed left-handed superhelices with similar sizes but opposite helicity to the right-handed superhelices of **R-1H-5%** (Fig. S13†). Additionally, when the doping ratio increased to 10% and 20%, the obtained **S-1H-10%** and **S-1H-20%** turned to right-handed superhelices (Fig. S13†). The opposite handedness inversion of **S-1H-x** to that of **R-1H-x**, as well as the identicality of components of **R**- and **S-1H-x** products which was determined by using the IR spectra, PXRD patterns (Fig. S14†), elemental analysis, ^{1}H-NMR spectra (Fig. S15–S17†), and EDX (Fig. S7†) and TG analyses (Fig. S8b†), confirmed the enantiomeric nature of **R**- and **S-1H-x** (x = 5%, 10%, 20%).

To further investigate the chiral properties of **R-1H-x** and **S-1H-x**, the circular dichroism (CD) measurements were performed on the solid-state samples. As shown in the CD spectra (Fig. S18†), all of **R-1H-x** exhibited positive dichroic signals in the range of 210–220 nm, and the signals of **S-1H-x** are opposite. These symmetrical signal peaks can be assigned to the n–π* transition of the P=O group. We had conjectured that the

introduction of an aromatic pempH$_2$ ligand may cause the appearance of a new CD signal in the higher wavelength range, but this is not observed in the spectra; instead, there is an unexplained weakening and a small blue shift of the signals of **R**- (or **S**-) **1H-x** ($x = 5\%$, 10%, 20%) compared to those of **R**- (or **S**-) **1H-0%** in the CD spectra. In addition, the circularly polarized luminescence (CPL) spectrum results (Fig. 3d) also demonstrated that **R**- and **S-1H-x** ($x = 5\%$, 10%, 20%) which were sensitized by pempH$_2$ ligands exhibit mirrored CPL signals at around 490 nm, 545 nm and 635 nm, corresponding to Tb^{3+} f–f transitions of $^5D_4 \rightarrow {}^7F_6$, $^5D_4 \rightarrow {}^7F_5$ and $^5D_4 \rightarrow {}^7F_3$, respectively. Their dissymmetric factors $|g_{lum}|$ were calculated to be in the range of 1–3×10^{-3}. The extra doping of the pempH$_2$ ligand did not cause a change in signal positivity or negativity since both CD and CPL spectra just reflected the molecular chirality in the system.

In contrast, vibrational circular dichroism (VCD) spectroscopy can probe conformational chirality and has been applied to study the supramolecular chirality of self-assemblies.[22] Therefore, the VCD spectrum is suitable for studying the effect of ligand doping on the macroscopic chirality of the superhelices. As shown in Fig. 3e, the solid-state VCD spectra exhibited the opposite symmetries of **R**- and **S-1H-x**, whereas their spectra differ with the doping ratio x. For **R**- and **S-1H-0%**, their VCD spectra exhibited opposite signal peaks at 1103, 1068, 1039, 1020 and 996 cm^{-1} as reported before, all of which are attributed to the stretching vibrations of the phosphonate group of ligands. The strongest VCD signal peak at 1020 cm^{-1} is negative for **R-1H-0%** and positive for **S-1H-0%**. Interestingly, although the peaks at 1020 cm^{-1} of **R**- and **S-1H-5%** have the same positive-negative signs as those of **R**- and **S-1H-0%**, the strength of the signals became much weaker, and the peak positions (1062, 1032, 1020 and 989 cm^{-1}) slightly differ from those of **R**- and **S-1H-0%** due to the incorporation of pempH$_2$ ligands. A remarkable difference was found for **R**- and **S-1H-10%**. Compared to **R**- and **S-1H-0%**, the strongest peak at 1020 cm^{-1} of **R-1H-10%** changed to be positive and that of **S-1H-10%** changed to be negative. The results are consistent with the handedness inversion phenomenon of the superhelices revealed by SEM images, *e.g.*, the macroscopic handedness of **R**- and **S-1H-0%** superhelices was preserved in **R**- and **S-1H-5%** but inversed in **R**- and **S-1H-10%**. Furthermore, the VCD spectra of

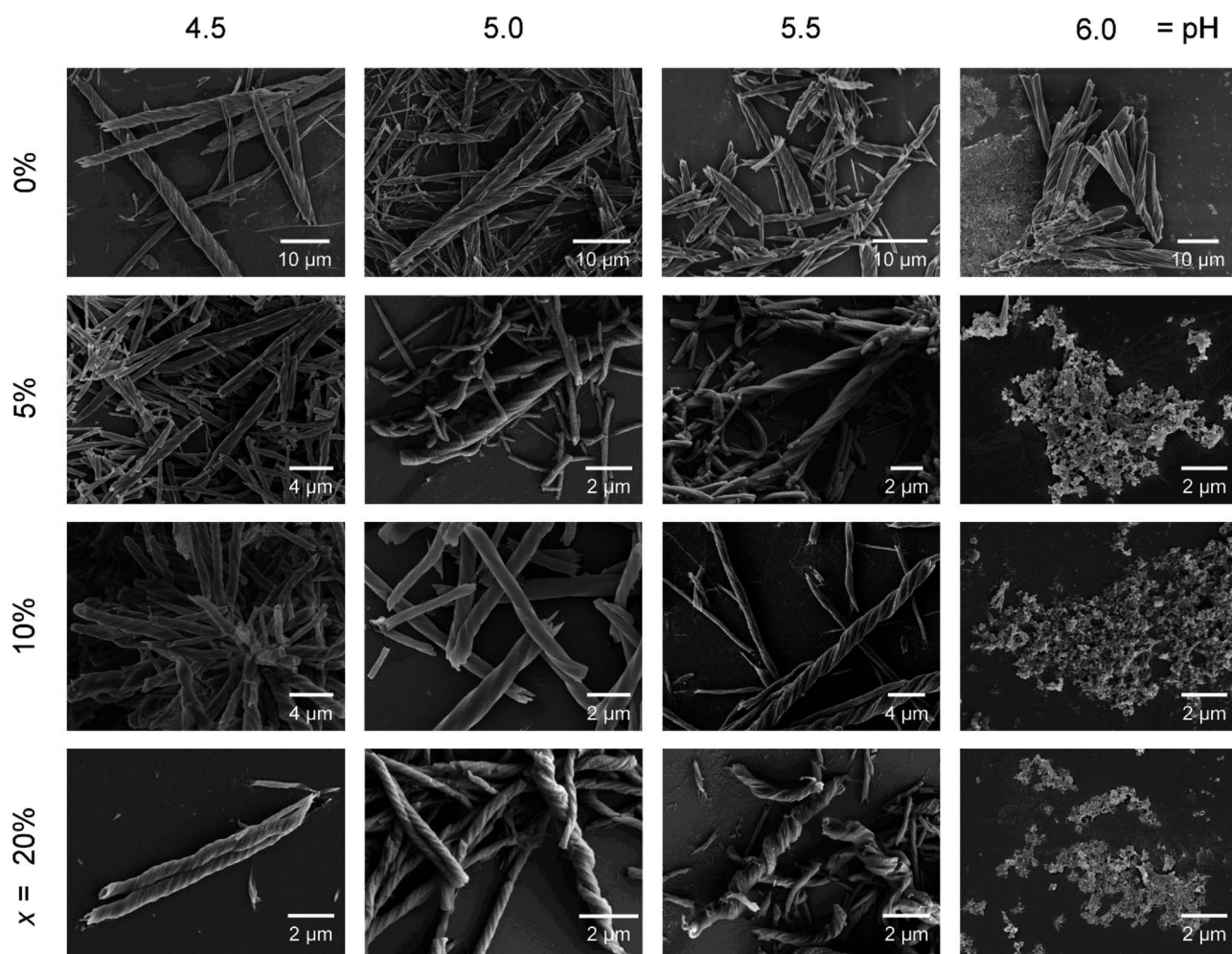**Fig. 4** SEM images of **R**-1H-x with different x values (0%, 5%, 10% and 20%) which are obtained at different pH values.

R- and *S*-1H-20% exhibited opposite signal peaks at 1056, 1017 and 996 cm^{-1}, similar to those of *R*- and *S*-1H-10% (1060, 1020 and 996 cm^{-1}) with the signal intensity just relatively weaker (Fig. S19†). To sum up, the VCD spectra revealed that the macroscopic handedness inversion phenomenon is closely related to the conformational chirality of the ligands in the *R*- and *S*-1H-*x* superhelices.

Influence of pH and temperature on helix morphologies

We then examined the effect of pH on the morphology of the helical products *R*-1H-*x*. The reactions were conducted similarly except for different pH values, and the products shared the same molecular-level structure, which was confirmed by the IR spectra and PXRD pattern (Fig. S20†). The SEM images show clearly that the products of *R*-1H-*x* (*x* = 5–20%) obtained at pH 6.0 are all microscale powder, unlike *R*-1H-0% which forms right-handed (*P*) superhelices at pH 4.3–6.5. For *R*-1H-5%, pure right-handed (*P*) superhelices were observed at pH 4.5–5.5. While for *R*-1H-10% and *R*-1H-20%, pure left-handed (*M*) superhelices formed at the same pH (Fig. 4, Table 2). It is interesting to note that when the pH was the same, for example at pH 4.5, the increase in doping amount of *R*-pempH$_2$ led to not only chirality inversion from right-handed (*x* = 5%) to left-handed (*x* = 10–20%) but also an obvious decrease in the pitch of the left-handed superhelices from 10% to 20%. Meanwhile, the increase in pH makes the "threads of the screws" of *R*-1H-*x* (*x* = 5–20%) stick out more perceptibly compared to the "grooves", especially for *R*-1H-20%, of which the products at pH 5.5 seem more like spirals rather than helical rods. The variety in morphology at different pH values can be explained by the degree of ligand deprotonation. The higher the pH and the degree of deprotonation, the easier it is for the ligand to bind to the Tb^{3+} ions, thus favouring the growth of the superhelices and making the "threads" more salient.

Additionally, the possible effect of temperature on the helix growth and handedness was also investigated through the same hydrothermal reaction for *x* = 5% and 10% at different temperatures (60–140 °C) while the pH was adjusted to 5.0. Likewise, the IR and PXRD spectra of *R*-1H-5% or *R*-1H-10%

generated at different temperatures were not significantly different (Fig. S21†). As for the morphology, similar to *R*-1H-0%, the 60 °C products were nanorods without a distinct helical morphology (Fig. S22†), while the superhelices could be obtained at a higher temperature of 80–120 °C. The handedness of the superhelices is maintained at different temperatures, with all *R*-1H-5% superhelices being right-handed (*P*) and all *R*-1H-10% superhelices being left-handed (*M*). However, when the temperature was increased to 140 °C, no superhelices but amorphous phases were obtained. The result suggests that the doping of *R*-pempH$_2$ ligands made it harder to form superhelices at higher temperatures.

It is noteworthy that for *R*-1H-5%, their size increased gradually as the reaction temperature increased from 80 °C to 120 °C (Fig. S23†). Compared to *R*-1H-5% produced at 100 °C, its length range decreased to 1–20 μm when prepared at 80 °C and increased to 10–30 μm when prepared at 120 °C. Similarly, the diameter range of the *R*-1H-5% product decreased to 0.1–1 μm at 80 °C but increased to 2–4 μm at 120 °C. In contrast, the morphology of the *R*-1H-10% left-handed helices at 80–120 °C showed little variation. This phenomenon implies that, among the products with different doping ratios, there may be differences in the intermolecular interactions that played a role in the superhelix growth process.

The proposed mechanism of the handedness inversion

The intriguing phenomenon of doping-induced handedness inversion in a coordination polymeric system, which has never been reported before to the best of our knowledge, persuaded us to investigate its mechanism. From the above-mentioned characterization, we can confirm that *R*-1H-*x* (*x* = 5–20%) superhelices retained a similar chain structure to that of *R*-1H-0% except that part of *R*-cyampH$^-$ in the chain was replaced by *R*-pempH$^-$ ligands. Therefore, we can attribute the handedness inversion from right-handed (*x* = 5%) to left-handed (*x* = 10%) to the effect of the doped *R*-pempH$^-$ ligand on this system.

As we previously proposed,[19] chiral transcription of homochiral 1D CPs from the molecular to the morphological level should meet at least two requirements. First, the interchain interactions must be sufficiently weak to prevent highly ordered and close packing of the helical chains. Second, a slight mismatch between neighboring chains provides a driving force to induce twisted packing of the chains. The two requirements are satisfactorily fulfilled for superhelices of *R*–Tb(cyampH)$_3$·3H$_2$O (*R*-1H-0%), in which the cyclohexyl groups hanging on the chains provide not only a weak van der Waals interaction between chains but also misalignment of the chains due to the fast interconversion of the conformers. However, factors determining the chirality of superhelices are more intriguing. The chirality of superhelices may inherit the same chirality of helical metal–organic chains, or *vice versa*. The latter phenomenon is similar to the hierarchical structure of collagen, in which the right-handed superhelix is composed of three polypeptides with a left-handed helical conformation.[23]

We envisage that although the interaction between chains is very weak, they play a crucial role in determining the chirality of

Table 2 The morphology of *R*-1H-*x* prepared at the same temperature (100 °C) but different pH values, or at the same pH (5.0) but different temperatures

Compound	pH = 4.5–5.5	pH = 6.0
R-1H-0%	Superhelix (*P*)	Superhelix (*P*)
R-1H-5%	Superhelix (*P*)	Powder
R-1H-10%	Superhelix (*M*)	Powder
R-1H-20%	Superhelix (*M*)	Powder
Compound	*T* = 80–120 °C	*T* = 140 °C
R-1H-0%	Superhelix (*P*)	Superhelix (*P*)
R-1H-5%	Superhelix (*P*)	Powder
R-1H-10%	Superhelix (*M*)	Powder

superhelices as well. For superhelices of R–Tb(cyampH)$_3$·3H$_2$O (R-**1H-0%**), van der Waals interactions are dominant between the R–Tb(cyampH)$_3$ chains. The resulting superhelix chirality (P) is the opposite of that of the single-chain to maximize van der Waals interaction. As for the R-**1H-x** system, the interchain interactions are slightly changed due to the doped R-pempH$^-$ ligand. Although the phenyl group of R-pempH$^-$ is similar in size to the cyclohexyl group in R-cyampH$^-$, it provides C–H⋯π interactions in addition to van der Waals interactions between chains (Fig. 5). When the doping is low (≤6%), the original van der Waals interaction between chains should be dominant. Therefore, right-handed (P) superhelices are observed for R-**1H-5%** as is the case for R-**1H-0%**. When the doping is high (≥9%), the C–H⋯π interaction associated with the phenyl groups of R-pempH$^-$ ligand becomes non-negligible. Therefore, left-handed (M) superhelices are found for R-**1H-10%** and R-**1H-20%**. More doped R-pempH$_2$ (x = 30% and 40%) will still produce left-handed superhelices as those in R-**1H-10%** (Fig. S24†). The results indicate that the additional C–H⋯π interaction enhances the interaction between the van der Waals chains, which is conducive for the superhelix to inherit the same chirality as the single metal–organic chain. This proposed mechanism is compatible with the effect of temperature on the

diameter of R-**1H-x**. Since van der Waals forces are susceptible to temperature, R-**1H-5%** exhibits an obvious temperature dependence on diameter similar to that of R-**1H-0%**,[19] while R-**1H-10%** containing more C–H⋯π interactions has almost the same size at different temperatures from 80 °C to 120 °C.

Influence of halogen-involving intermolecular interactions on the handedness inversion

To further explore the effect of interchain interactions on the morphology and chirality of the Tb/R-cyampH$_2$ system, we tried to introduce other interactions into the system by doping halogen-substituted pempH$_2$ (XpempH$_2$, X = F, Cl, Br)[24] ligands using a similar strategy, where the introduced halogen atoms can participate in C–H⋯X interactions. The doped superhelices were synthesized at pH 5.0 under the same conditions as R-**1H-x**. As shown in Fig. 6 and Table 3, the obtained superhelices of R-**2F-5%** are right-handed and those of R-**2F-10%** are left-handed, indicating that the R-FpempH$_2$ ligand has a similar effect on the helical sense of R-**2F-x** as the R-pempH$_2$ ligand does.

The pattern of handedness inversion still held up in the R-**3Cl-x** system, but a slight inconstancy emerged. R-**3Cl-5%** was formed as right-handed superhelices; however, as the doping ratio of R-ClpempH$_2$ increased to 10%, although left-handed superhelices became predominant in R-**3Cl-10%**, right-handed helical ends appeared in a small portion of the left-handed helices (Fig. 6). Nonetheless, the majority of the helical products are left-handed as for R-**3Cl-10%**, showing that R-ClpempH$_2$ still has a similar ability to invert handedness as R-pempH$_2$ and R-FpempH$_2$ do.

Nonetheless, when it came to R-BrpempH$_2$, the case became quite different. R-**4Br-5%** helices are as right-handed as R-**1H-5%**; oddly, most of the superhelices of R-**4Br-10%** were still right-handed (Fig. 6). We originally suspected that due to the relatively low solubility of BrpempH$_2$, it might have difficulty entering the coordination polymer during the reaction, causing

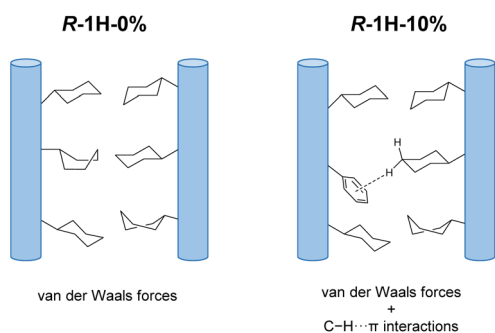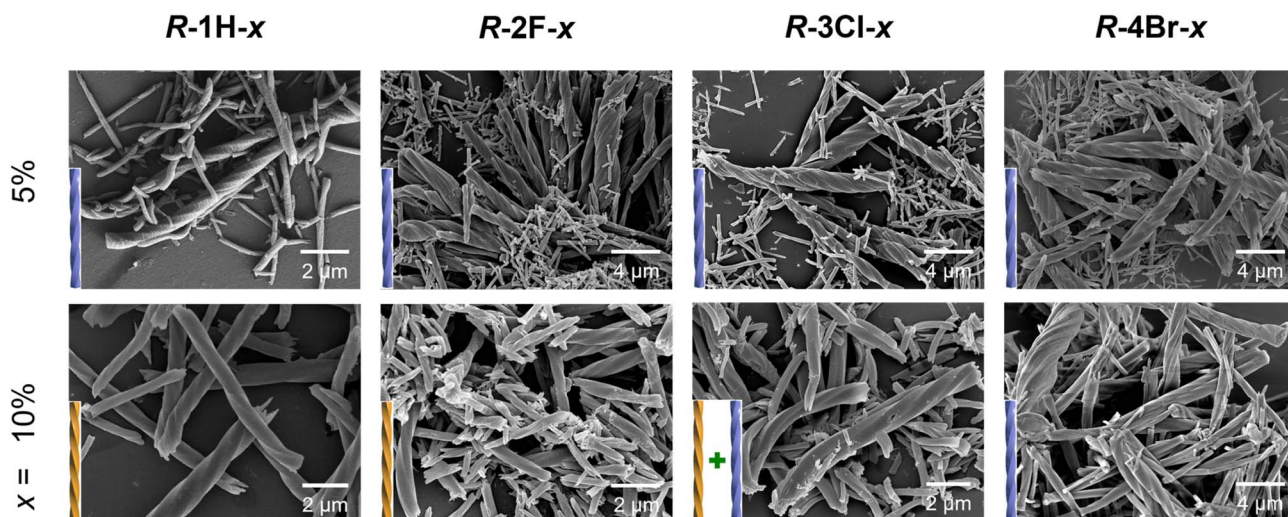**Fig. 5** The weak interchain interactions in the R-**1H-x** system.

Fig. 6 SEM images of R-**1H-x**, R-**2F-x**, R-**3Cl-x**, and R-**4Br-x** with different x values (5% and 10%) which are obtained at pH = 5.0 and 100 °C.

Table 3 The actual formulae and morphology of compounds *R*-2F-*x*, *R*-3Cl-*x* and *R*-4Br-*x* obtained at pH 5.0 and 100 °C. The ratios of the two ligands were calculated by using the integrals of signal peaks in their ^{1}H-NMR spectra

Compound	The actual formula	Ratio[a] (*a*)	Handedness	Diameter (μm)	Length (μm)
***R*-1H-0%**	Tb(*R*-cyampH)$_3$	0%	Superhelix (*P*)	2–7	40–100
***R*-2F-5%**	Tb(*R*-cyampH)$_{2.87}$(*R*-FpempH)$_{0.13}$·3H$_2$O	4.4%	Superhelix (*P*)	0.2–2	2–20
***R*-2F-10%**	Tb(*R*-cyampH)$_{2.71}$(*R*-FpempH)$_{0.29}$·3H$_2$O	9.7%	Superhelix (*M*)	0.2–2	2–20
***R*-3Cl-5%**	Tb(*R*-cyampH)$_{2.87}$(*R*-ClpempH)$_{0.13}$·3H$_2$O	4.2%	Superhelix (*P*)	0.2–2	2–20
***R*-3Cl-10%**	Tb(*R*-cyampH)$_{2.73}$(*R*-ClpempH)$_{0.27}$·3H$_2$O	8.9%	Superhelix (*M* + *P*)[b]	0.2–2	2–15
***R*-4Br-5%**	Tb(*R*-cyampH)$_{2.89}$(*R*-BrpempH)$_{0.11}$·3H$_2$O	3.8%	Superhelix (*P*)	0.2–2	3–15
***R*-4Br-10%**	Tb(*R*-cyampH)$_{2.64}$(*R*-BrpempH)$_{0.36}$·3H$_2$O	12.1%	Superhelix (*P*)	0.2–4	2–15

[a] The ratio is determined by using the ^{1}H NMR spectra. [b] The left-handed (*M*) product is dominant.

the actual ratio (*a*) of BrpempH$_2$ in the superhelix to be lower than the doping ratio (*x*). However, this conjecture was disproved by the ^{1}H-NMR detection results (Fig. S24–S29†). Moreover, the EDX (Fig. S30†) and TG (Fig. S31–S33†) analyses of ***R*-2F-*x*, *R*-3Cl-*x*** and ***R*-4Br-*x*** further confirm that they have similar formulae, which are listed in Table 3, to ***R*-1H-*x***.

Obviously, the handedness inversion of the *R*-XpempH$_2$-doped superhelices is highly dependent on the halogen substitute. ***R*-2F-*x*** undergoes a complete handedness inversion from right-handed (*P*) to left-handed (*M*) when the *x* value increases from 5% to 10%, whereas ***R*-4Br-*x*** superhelices retain the same right-handedness when *x* = 5–10%. For ***R*-3Cl-*x***, chirality inversion from *P* to *M* is not complete with the *M*-superhelix being the dominant phase at *x* = 10%. Noting that the *R*-XpempH$_2$-doped superhelices show nearly identical PXRD patterns and IR spectra to ***R*-1H-*x*** (Fig. S34 and S35†), they should possess similar chain structures except for different halogen substitutes in the doped ligand. We propose that at *x* = 10%, the interchain interaction associated with the *R*-XpempH$^-$ ligand is non-negligible. The presence of a halogen atom may introduce C–H⋯X (X = F, Cl, Br) interaction in addition to the van der Waals and possible C–H⋯π interactions. Since the strength of C–H⋯X interaction decreases with decreasing electronegativity of X in the sequence: F > Cl > Br, the chirality inversion of ***R*-2F-*x*** from *P* (*x* = 5%) to *M* (*x* = 10%) is attributed to the enhanced interaction between chains *via* C–H⋯F interactions. As for ***R*-4Br-*x***, the C–H⋯Br interaction is very weak and the van der Waals contact could still dominate between chains even when the doping content is above *x* = 10%. As a result, right-handed (*P*) superhelices are observed in both ***R*-4Br-5%** and ***R*-4Br-10%**. In the case of ***R*-3Cl-*x***, the strength of C–H⋯Cl interaction is between that of C–H⋯F and C–H⋯Br, which may explain the incomplete handedness inversion of the ***R*-3Cl-*x*** superhelices when *x* increases from 5% to 10%.

significantly different, but their morphologies are significantly influenced by the doping ratio (*x*) of the homochiral ligand, with ***R*-1H-*x*** being right-handed when *x* ≤ 6% and left-handed when *x* ≥ 9%. For ***S*-1H-*x***, the products have a handedness exactly opposite to the ***R*-1H-*x*** superhelices. We propose that the C–H⋯π interactions introduced by the pempH$_2$ ligand enhance the interchain interactions and thus make superhelices, at a higher doping ratio, maintain their handedness during coordination polymeric chain stacking with each other, unlike in ***R*-** and ***S*-1H-0%** where superhelices are generated with opposite handedness to the coordination polymeric helical chain. To verify our deduction, we replaced *R*-pempH$_2$ with halogen-substituted *R*-XpempH$_2$, introducing C–H⋯X interactions into the system to obtain similar *R*–Tb(cyamp)$_{3(1-a)}$(Fpemp)$_{3a}$·3H$_2$O (***R*-2F-*x***), *R*–Tb(cyamp)$_{3(1-a)}$(Clpemp)$_{3a}$·3H$_2$O (***R*-3Cl-*x***), and *R*–Tb(cyamp)$_{3(1-a)}$(Brpemp)$_{3a}$·3H$_2$O (***R*-4Br-*x***) and found that handedness inversion phenomena exist in ***R*-2F-*x*** and ***R*-3Cl-*x***, where interchain interactions are stronger, but cannot occur in ***R*-4Br-*x*** with weaker C–H⋯Br interchain interactions, thus rationalizing our proposed mechanism. The above finding is the first example of handedness inversion caused by doping of homochiral ligands, which could provide new ideas for the design of chirality or handedness controllable self-assembled systems and may contribute to the development of novel coordination polymeric materials with helical morphologies.

Conflicts of interest

There are no conflicts to declare.

Data availability

The experimental data have been provided in the ESI.†

Conclusions

In this work, we introduced *R*- or *S*-pempH$_2$ in different ratios into *R*- or *S*–Tb(cyamp)$_3$·3H$_2$O (***R*-** and ***S*-1H-0%**), respectively, to obtain a series of coordination polymeric products *R*- or *S*–Tb(cyamp)$_{3(1-a)}$(pemp)$_{3a}$·3H$_2$O (***R*-** and ***S*-1H-*x***) with superhelical morphologies. In the range of *x* = 0–20%, the coordination and crystal structures of ***R*-** and ***S*-1H-*x*** at the molecular level are not

Author contributions

C.-Y. W. performed the experiments and wrote the manuscript. J.-G. J. assisted in directing the synthesis and characterization. G.-G. W. assisted in directing the synthesis of the helix. M.-F. Q. assisted in NMR measurements. K. X. assisted in luminescence measurements. L.-M. Z. conceived the project and revised the manuscript.

Acknowledgements

Notes and references

1 (a) Y. Timsit, *Int. J. Mol. Sci.*, 2013, **14**, 8252; (b) S. C. Ha, K. Lowenhaupt, A. Rich, Y. Kim and K. K. Kim, *Nature*, 2005, **437**, 1183; (c) B. Fu, J. Huang, Y. Chen, Y. Wang, T. Xue, G. Xu, S. Wang and X. Zhou, *Chem. Commun.*, 2016, **52**, 10052; (d) J. Skolnick, H. Zhou and M. Gao, *Proc. Natl. Acad. Sci. U. S. A.*, 2019, **116**, 26571; (e) H. Miyake, H. Kamon, I. Miyahara, H. Sugimoto and H. Tsukube, *J. Am. Chem. Soc.*, 2008, **130**, 792; (f) I. Usov, J. Adamcik and R. Mezzenga, *ACS Nano*, 2013, **7**, 10465.

2 (a) H. Jintoku, M. Takafuji, R. Odac and H. Ihara, *Chem. Commun.*, 2012, **48**, 4881; (b) T. Noguchi, B. Roy, D. Yoshihara, J. Sakamoto, T. Yamamoto and S. Shinkai, *Angew. Chem., Int. Ed.*, 2017, **56**, 12518; (c) R. Sethy, J. Kumar, R. Métivier, M. Louis, K. Nakatani, N. M. T. Mecheri, A. Subhakumari, K. G. Thomas, T. Kawai and T. Nakashima, *Angew. Chem., Int. Ed.*, 2017, **56**, 15053.

3 (a) M. Raynal, F. Portier, P. W. N. M. van Leeuwen and L. Bouteiller, *J. Am. Chem. Soc.*, 2013, **135**, 17687; (b) Z.-C. Shen, Y.-T. Sang, T.-Y. Wang, J. Jiang, Y. Meng, Y.-Q. Jiang, K. Okuro, T. Aida and M.-H. Liu, *Nat. Commun.*, 2019, **10**, 3976.

4 (a) S. Lee, K. Y. Kim, S. H. Hung, J. H. Lee, M. Yamada, R. Sethy, T. Kawai and J. H. Jung, *Angew. Chem., Int. Ed.*, 2019, **58**, 18878; (b) Z.-L. Gong, X. Zhu, Z. Zhou, S.-W. Zhang, D. Yang, B. Zhao, Y.-P. Zhang, J. Deng, Y. Cheng, Y.-X. Zheng, S.-Q. Zang, H. Kuang, P. Duan, M. Yuan, C.-F. Chen, Y.-S. Zhao, Y.-W. Zhong, B.-Z. Tang and M. Liu, *Sci. China: Chem.*, 2021, **64**, 2060–2104; (c) C. Liu, J.-C. Yang, J. W. Y. Lam, H.-T. Feng and B.-Z. Tang, *Chem. Sci.*, 2022, **13**, 611–632.

5 (a) Z.-Y. Lv, Z.-H. Chen, K.-N. Shao, G.-Y. Qing and T.-L. Sun, *Polymers*, 2016, **8**, 310; (b) X.-Q. Dou, N. Mehwish, C.-L. Zhao, J.-Y. Liu, C. Xing and C.-L. Feng, *Acc. Chem. Res.*, 2020, **53**, 852; (c) L. Zhang, H.-X. Wang, S. Li and M.-H. Liu, *Chem. Soc. Rev.*, 2020, **49**, 9095.

6 (a) F. Wang, M.-G. Qin, T. Peng, X.-H. Tang, A. Y. Dang-i and C.-L. Feng, *Langmuir*, 2018, **34**, 7869; (b) Q. Ye, F. Zheng, E.-Q. Zhang, H. K. Bisoyi, S.-Y. Zheng, D.-D. Zhu, Q.-H. Lu, H.-L. Zhang and Q. Li, *Chem. Sci.*, 2020, **11**, 9989.

7 A. Kousar, J. Liu, N. Mehwish, F. Wang, A. Y. Dang-i and C. Feng, *Mater. Today Chem.*, 2019, **11**, 217.

8 (a) G.-F. Liu, L.-Y. Zhu, W. Ji, C.-L. Feng and Z.-X. Wei, *Angew. Chem., Int. Ed.*, 2016, **55**, 2411; (b) G.-F. Liu, J.-H. Sheng, H.-W. Wu, C.-L. Yang, G.-B. Yang, Y.-X. Li, R. Ganguly, L.-L. Zhu and Y.-L. Zhao, *J. Am. Chem. Soc.*, 2018, **140**, 6467.

9 (a) F. Wang and C. Feng, *Angew. Chem., Int. Ed.*, 2018, **57**, 5655; (b) X.-L. Zha, Y.-L. Chen, H. Fan, Y.-G. Yang, Y. Xiong, G.-L. Xu, K. Yan, Y.-D. Wang, Y. Xie and D. Wang,

Angew. Chem., Int. Ed., 2021, **60**, 7759; (c) G.-F. Liu, J.-H. Sheng, W. L. Teo, G.-B. Yang, H.-W. Wu, Y.-X. Li and Y.-L. Zhao, *J. Am. Chem. Soc.*, 2018, **140**, 16275.

10 M. Go, H. Choi, K. Y. Kim, C. J. Moon, Y. Choi, H. Miyake, S. S. Lee, S. H. Jung, M. Y. Choi and J. H. Jung, *Org. Chem. Front.*, 2019, **6**, 1100.

11 (a) J.-X. Cui, A.-H. Liu, Y. Guan, J. Zheng, Z.-H. Shen and X.-H. Wan, *Langmuir*, 2010, **26**, 3615; (b) Q.-Y. Deng, E.-B. Zhou, Y.-W. Huang, W.-X. Qing, H.-Y. Zhai, Z.-H. Liu and Z.-X. Wei, *Chem. Commun.*, 2019, **55**, 4379.

12 (a) Y. Yang, J. Liang, F. Pan, Z. Wang, J. Zhang, K. Amin, J. Fang, W. Zou, Y. Chen, X. Shi and Z. Wei, *Nat. Commun.*, 2018, **9**, 3808; (b) M. Kumar, P. Brocorens, C. Tonnelé, D. Beljonne, M. Surin and S. J. George, *Nat. Commun.*, 2014, **5**, 5793.

13 (a) Z. Geng, Y. Zhang, Y. Zhang, Y. Li, Y. Quan and Y. Cheng, *J. Mater. Chem. C*, 2021, **9**, 12141–12147; (b) Z. Wang, A. Hao and P. Xing, *Angew. Chem., Int. Ed.*, 2023, **62**, e202214504.

14 (a) F. Wang and C.-L. Feng, *Chem.–Eur. J.*, 2018, **24**, 1509; (b) N. Katsonis, F. Lancia, D. A. Leigh, L. Pirvu, A. Ryabchun and F. Schaufelberger, *Nat. Chem.*, 2020, **12**, 939–944; (c) J. Chen, C. Yang, S. Ma, Z. Liu, W. Xiang and J. Zhang, *Chem. Sci.*, 2023, **14**, 2091–2096.

15 (a) S. R. Batten, *Curr. Opin. Solid State Mater. Sci.*, 2001, **5**, 107; (b) S. Kitagawa, R. Kitaura and S. I. Noro, *Angew. Chem., Int. Ed.*, 2004, **43**, 2334; (c) Y. Liu and Z. Tang, *Chem.–Eur. J.*, 2012, **18**, 1030; (d) J. Dong, Y. Liu and Y. Cui, *Acc. Chem. Res.*, 2021, **54**, 194; (e) S. Dhers, H. L. C. Feltham and S. Brooker, *Coord. Chem. Rev.*, 2015, **296**, 24; (f) G. Givaja, P. Amo-Ochoa, C. J. Gómez-García and F. Zamora, *Chem. Soc. Rev.*, 2012, **41**, 115; (g) M. Lippi and M. Cametti, *Coord. Chem. Rev.*, 2021, **430**, 213661.

16 (a) L. Han and M.-C. Hong, *Inorg. Chem. Commun.*, 2005, **8**, 406; (b) H. M. Tay, N. Kyratzis, S. Thoonen, S. A. Boer, D. R. Turner and C. Hua, *Coord. Chem. Rev.*, 2021, **435**, 213763; (c) G.-G. Weng and L.-M. Zheng, *Sci. China: Chem.*, 2020, **63**, 619–636; (d) Y. Xu, Y.-S. Yu, X.-D. Huang, S.-S. Bao, H.-m. Ding, Y.-q. Ma and L.-M. Zheng, *Inorg. Chem.*, 2018, **57**, 12143–12154.

17 (a) S.-Y. Zhang, S.-Y. Yang, J.-B. Lan, S.-J. Yang and J.-S. You, *Chem. Commun.*, 2008, 6170; (b) C. Li, K. Deng, Z.-Y. Tang and L. Jiang, *J. Am. Chem. Soc.*, 2010, **132**, 8202; (c) K. Hirai, B. Yeom and K. Sada, *ACS Nano*, 2017, **11**, 5309; (d) G.-G. Weng, X.-D. Huang, R. Hu, S.-S. Bao, Q. Zou, G.-H. Wen, Y.-Q. Zhang and L.-M. Zheng, *Chem.–Asian J.*, 2021, **16**, 2648–2658.

18 (a) J. Huang, H.-M. Ding, Y. Xu, D. Zeng, H. Zhu, D.-M. Zang, S.-S. Bao, Y.-Q. Ma and L.-M. Zheng, *Nat. Commun.*, 2017, **8**, 2131; (b) L.-Q. Wu, Y. Xu, T. Hou, J.-G. Jia, X.-D. Huang, G.-G. Weng, S.-S. Bao and L.-M. Zheng, *Chem.–Eur. J.*, 2021, **27**, 16722; (c) T. Hou, L.-Q. Wu, Y. Xu, S.-S. Bao and L.-M. Zheng, *Molecules*, 2023, **28**, 163.

19 G.-G. Weng, B.-K. Hong, S.-S. Bao, Y.-J. Wen, L.-Q. Wu, X.-D. Huang, J.-G. Jia, G.-H. Wen, S.-H. Li, L.-M. Peng and L.-M. Zheng, *Chem. Sci.*, 2021, **12**, 12619.

20 Z.-S. Cai, S.-S. Bao, M. Ren and L.-M. Zheng, *Chem.–Eur. J.*, 2014, **20**, 17137–17142.

21 *TOPAS, version 5.0*, Bruker AXS Inc., Madison, WI, 2014.

22 (*a*) J. Gao, Y. Okazaki, E. Pouget, S. Nlate, B. Kauffmann, F. Artzner, T. Buffeteau and R. Oda, *Mater. Chem. Front.*, 2021, **5**, 3021; (*b*) B. Martial, T. Lefèvre, T. Buffeteau and M. Auger, *ACS Nano*, 2019, **13**, 3232.

23 J. Engel and H. P. Bächinger, *Top. Curr. Chem.*, 2005, **247**, 7.

24 J.-G. Jia, C.-C. Zhao, S.-S. Bao, L.-Q. Wu, G.-H. Wen, A. J. Jacobson, J. Ma and L.-M. Zheng, *J. Am. Chem. Soc.*, 2021, **143**, 17587–17598.